From Direct Current to Generated Pattern Current: Temporal Energy Structuring as the Third Axis of Electrochemical Optimization

Ibrahim Karakoc

GigaPulse Energy, Izmir, Turkey | *ibrahim@gigapulse.energy*

PCT/TR2025/051176 | USPTO Appl. No. 19/298,223 | Priority: July 23, 2025

Summary

Electrochemical process control relies on constant-current and constant-voltage protocols that regulate energy magnitude but ignore its temporal structure. Since electrochemical interfaces are nonlinear, Jensen's inequality dictates that identical average current delivered in different temporal patterns produces different outcomes. The Generated Pattern Current (GPC) framework introduces temporal structure as an explicit control parameter: current is delivered through normalized shape functions matched to interfacial timescales. In battery formation, this reduces process time by 50–70% while improving solid-electrolyte interphase quality. In water electrolysis, cell overpotential decreases by approximately 11% at equivalent production rates. In charging infrastructure, grid peak demand drops by 40% through multi-source pattern coordination. These gains require no hardware changes — only firmware updates to existing power electronics. Application across more than 15 electrochemical sectors demonstrates that temporal energy structuring is a universal, hardware-agnostic optimization dimension complementary to advances in materials and cell design.

Context & Scale

Electrochemical technologies — batteries, electrolyzers, fuel cells, and electrochemical manufacturing — collectively represent a multi-trillion-dollar industrial base central to the global energy transition. Process control in these systems has remained fundamentally unchanged for over two centuries: constant current or voltage, occasionally interrupted by simple rectangular pulses. Yet every electrochemical interface of practical interest is nonlinear, meaning that process outcomes depend not only on how much energy is delivered but on how that energy is distributed in time.

The Generated Pattern Current framework addresses this gap by introducing a new control dimension — temporal energy structure — that is orthogonal to and compatible with existing optimization of materials, electrolytes, and cell geometry:

1. Quantified industrial impact: Battery formation time reduced 50–70%, electrolysis overpotential reduced ~11%, charging station grid demand reduced ~40% — all at identical average current and total energy [1].

2. Hardware-agnostic deployment: The framework modifies only the current control algorithm. Gigafactory formation lines, MW-scale electrolyzers, and industrial plating baths can adopt it through firmware updates to existing power electronics [1].

3. Theoretical foundation: Jensen's inequality applied to Butler-Volmer kinetics, nucleation theory, and mass transport establishes that temporal structuring is a first-order effect in nonlinear electrochemical systems, not a perturbative correction [12,13].

4. Cross-domain universality: The principle applies across more than 15 sectors from battery formation to fusion energy, defense, and space technologies, demonstrated in an accompanying paper series. The common mechanism is temporal pattern interaction with multi-scale interfacial dynamics [1].

1. Introduction

The electrochemical interface evolves across multiple timescales simultaneously. Double-layer charging operates on microseconds [12]. Solid-electrolyte interphase (SEI) films nucleate and grow over minutes to hours [3,4,7]. Diffusion layers build and collapse on millisecond-to-second timescales [12,13]. Temperature gradients develop and dissipate over seconds to minutes. Conventional control — constant current (CC), constant voltage (CV), or the concatenated CC-CV protocol — applies a fixed excitation regardless of this dynamic complexity [2,5,8,9].

This approach reflects an implicit assumption: that system response is proportional to average current. For linear systems this holds. For the nonlinear systems governing real electrochemical interfaces — Butler-Volmer kinetics [12], diffusion-limited transport [13], nucleation with exponential supersaturation dependence [16] — it does not. For any nonlinear function f, Jensen's inequality establishes that f(mean(x)) ≠ mean(f(x)). Two protocols delivering identical average current and total energy therefore produce different electrochemical states.

Pulse electrolysis partially recognized this in the mid-20th century [14,15], but its design space is limited to rectangular on-off waveforms with three parameters (amplitude, on-time, off-time). The Generated Pattern Current (GPC) framework, introduced here, generalizes this insight: the full temporal structure of current delivery is a designable control variable with the same status as magnitude, chemistry, and geometry [1]. A battery cell with optimized cathode chemistry is further improved by optimizing how current is delivered during formation. An electrolyzer with state-of-the-art catalysts achieves lower overpotential through temporal structuring. No new hardware, materials, or electrolytes are required — only a GPC controller module connected to the current and voltage inputs of existing power sources.

The practical stakes are substantial. Battery formation alone consumes 30–40% of gigafactory energy and 20–30% of total production time [34,37]. Water electrolysis faces a voltage efficiency gap of 0.4–0.8 V above the thermodynamic minimum, largely attributable to kinetic and mass-transport overpotentials that scale nonlinearly with current density [17]. EV charging infrastructure must reconcile fast per-vehicle charge rates with grid capacity constraints that tighten as fleet electrification accelerates [8,10]. In each case, the nonlinearity of the underlying electrochemical processes means that how current is delivered matters independently of how much current is delivered. A framework that systematically exploits this degree of freedom addresses all three bottlenecks simultaneously.

This perspective presents the theoretical basis, defines the mathematical framework, demonstrates cross-domain applicability, and outlines a research agenda. The supporting patent [1] and a 15-paper companion series provide domain-specific analyses.

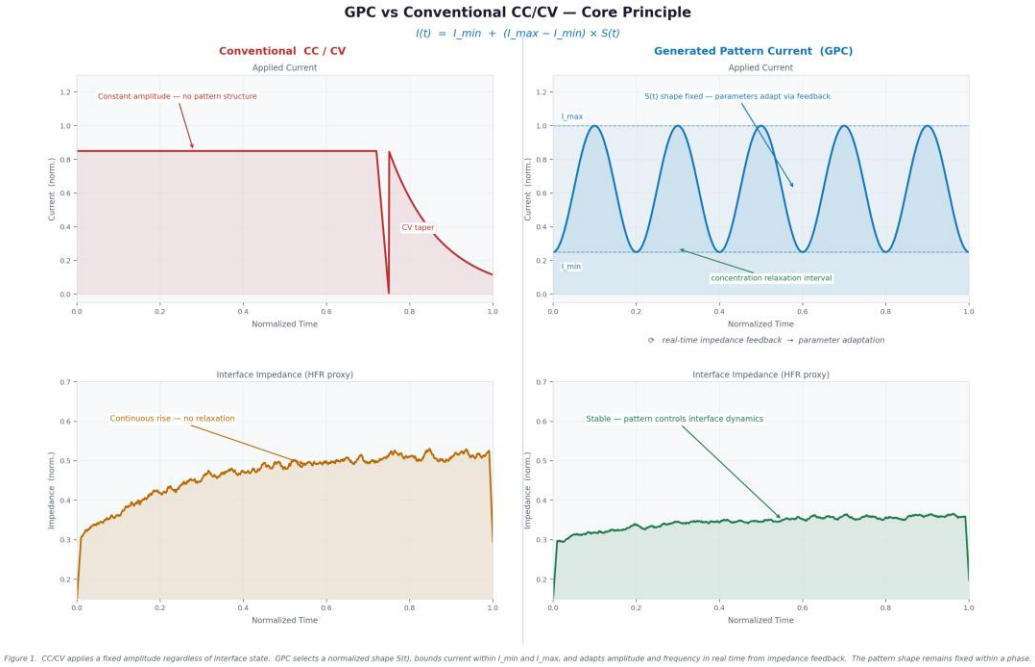

Figure 1. Conventional CC/CV (left) applies fixed amplitude regardless of interface state; impedance rises monotonically. Generated Pattern Current (right) delivers current through a normalized shape function S(t) bounded between I_min and I_max, adapting scaling parameters via impedance feedback while preserving pattern geometry. Interface impedance remains controlled through periodic relaxation matched to interfacial timescales.

2. The Generated Pattern Current Framework

2.1 Core Principle

A pattern is defined by a normalized shape function S(t) ∈ [0,1], a lower bound I_min > 0, and an upper bound I_max. The delivered current is [1]:

$$I(t) = I_{min} + (I_{max} - I_{min}) \times S(t) \qquad (1)$$

The shape function encodes temporal structure independently of amplitude: changing I_max scales the current without altering pattern geometry. I_min is maintained above zero to prevent uncontrolled open-circuit drift. The pattern library includes eight built-in types — Sinusoidal, Superpulse, Tangential, Parabola, Bezier, Triangle, Trapezoid, and Sigmoid — each targeting different electrochemical dynamics (Figure 2). The ChemPat synthesis mode generates patterns directly from electrode kinetic parameters encoded in chemistry calibration files, moving from empirical selection toward physics-informed pattern design [1].

2.2 Pattern Library

Each built-in type targets specific electrochemical dynamics. The Sinusoidal pattern provides smooth, periodic excitation suitable for systems sensitive to abrupt current transitions. Superpulse delivers multi-level rectangular current with two or more distinct plateaus per period, maintaining non-zero current at all times while providing aggressive temporal contrast. The Tangential pattern features rapid transitions for processes requiring sharp mass transport disruption. The Parabola offers symmetric excitation with gradual onset and offset, minimizing dI/dt stress. Bezier curves enable asymmetric control of rise and fall characteristics independently. The Triangle pattern provides uniform dI/dt throughout the cycle, useful for impedance characterization. The Trapezoid sustains high-current plateaus with controlled transitions, representing the closest analog to conventional pulse electrolysis but with continuously variable parameters. The Sigmoid provides asymmetric S-shaped transitions effective for nucleation-sensitive formation phases [1].

Beyond the built-in library, the ChemPat synthesis mode generates patterns directly from electrochemical models. A chemistry calibration file (.gpchei format) encodes the target system's electrode kinetics parameters, mass transport coefficients, and interfacial growth models. ChemPat computes a shape function whose temporal characteristics are matched to the system's intrinsic timescales — moving from empirical pattern selection toward physics-informed pattern design. The library is architecturally unbounded: any analytically defined or data-driven normalized shape function qualifies as a GPC pattern, provided it satisfies S(t) in [0, 1] and is continuously defined over the pattern period [1].

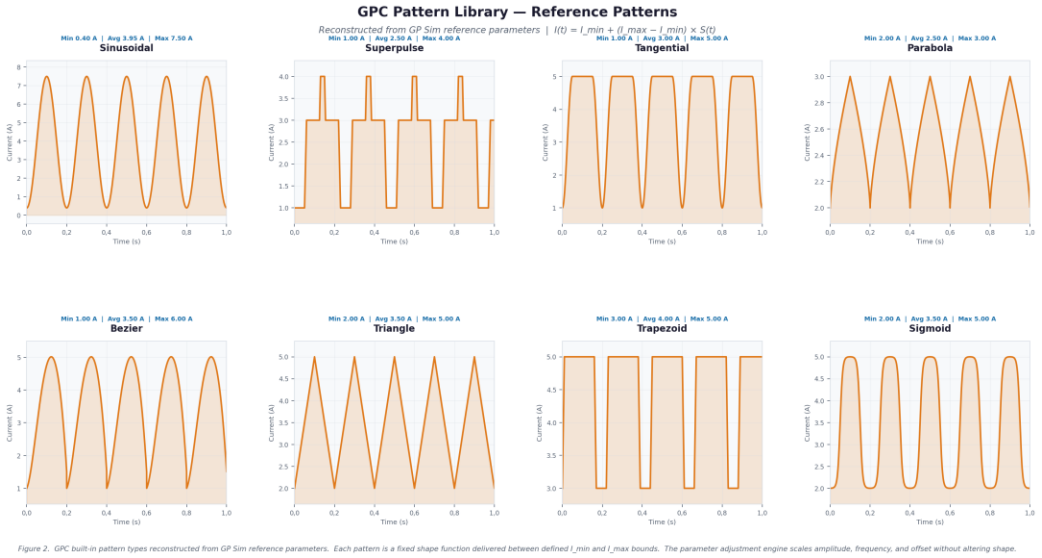

Figure 2. Built-in pattern types reconstructed from reference parameters. Each is a normalized shape function S(t) delivered between I_min and I_max. The parameter adjustment engine scales amplitude, frequency, and offset without altering shape geometry.

2.3 Stress and Performance Metrics

A composite stress index quantifies electrochemical burden per unit process progress [1]:

$$S_{gpc} = (I_{RMS}/I_{ref})^{\alpha} \times f_T \times f_{mode} \times f_{slew} \times f_{phase} \times f_{th} \qquad (2)$$

Each factor is dimensionless and bounded. The amplitude term (I_RMS/I_ref)^alpha captures current intensity relative to a reference; RMS current is used because it correlates with resistive

heating and electrochemical stress more accurately than peak or average values. f_T is the temperature correction factor, normalizing stress to a reference temperature through Arrhenius-type scaling. f_mode captures the shape-dependent stress reduction relative to equivalent DC — the factor that makes GPC fundamentally different from CC: a pattern that includes relaxation intervals within each period reduces interfacial stress even at identical RMS current [1]. f_slew penalizes excessive current transition rates (dI/dt) that can induce transient overpotentials exceeding steady-state values. f_phase accounts for multi-source phase relationships: constructive interference between sources can produce instantaneous current peaks exceeding individual source limits, while anti-phase coordination reduces peak aggregate current. f_th incorporates thermal feedback — if measured temperature exceeds a threshold, f_th increases the stress index, triggering adaptive parameter response [1].

2.4 Feedback Architecture

The framework operates as a closed loop. The feedback interface acquires voltage, current, temperature, and impedance at rates appropriate to the application — kilohertz for battery formation, lower rates for industrial electrolysis. Pattern parameters (I_min, I_max, frequency) adapt in real time based on feedback, while the pattern shape S(t) remains fixed within each process phase. This separation ensures temporal structure is preserved even as conditions change. Phase transitions occur at predefined state-of-charge, impedance, or time thresholds — when triggered, the shape function itself changes to match the new process phase requirements [1].

2.5 Multi-Source Synchronization

Multi-source configurations add a synchronization layer for systems involving multiple current sources. Three modes are defined: in-phase synchronization maximizes peak current delivery; anti-phase synchronization offsets patterns to minimize peak aggregate current and grid impact while maintaining average delivery rate; and complementary synchronization combines different patterns to produce aggregate temporal structures that no single source could achieve alone. The synchronization layer interacts with the stress index through f_phase, ensuring that multi-source interference effects are accounted for in the overall stress calculation. This architecture enables coordinated GPC operation from milliwatt biomedical devices to megawatt energy stations [1].

3. Energy Distribution Theory

In conventional electrochemical control, the implicit assumption is that the system response is proportional to the average current delivered. Under this assumption, two current protocols delivering the same total energy $E = \int V(t)I(t)dt$ over the same duration are expected to produce equivalent electrochemical outcomes. This would be correct if the system were linear — that is, if the response at each instant were proportional to the instantaneous current. However, electrochemical interfaces are governed by fundamentally nonlinear processes that invalidate this assumption.

The Butler-Volmer equation describes charge transfer as an exponential function of overpotential [12]:

$$j = j_0[\exp(\alpha n F\eta/RT) - \exp(-(1-\alpha)nF\eta/RT)] \quad (3)$$

Diffusion-limited transport adds square-root time dependence through the Cottrell equation [12,13]. Nucleation rates depend doubly-exponentially on overpotential through classical nucleation theory [16]. None of these respond linearly to current excitation. For any nonlinear response function f:

$$f(\text{mean}(x)) \neq \text{mean}(f(x)) \quad (4)$$

This inequality — known as Jensen's inequality — is mathematically exact for any strictly convex or concave function and is not an approximation. Applied to electrochemical systems, it means that the response to a constant current equal to the mean of a time-varying profile is not the same as the time-averaged response to the time-varying profile itself. Two current protocols with identical average current and identical total energy produce different interface states, different film morphologies, different product distributions, and different degradation rates. The temporal structure of current delivery is not a second-order perturbative correction — it is a first-order determinant of the electrochemical outcome.

$$\text{Response} = F(E, S_t, M) \quad (5)$$

where E is total energy, S_t is the temporal structure (how energy is distributed in time), and M represents material and geometric parameters. Conventional control optimizes E and M while treating S_t as irrelevant — effectively fixing it at the constant-current identity. The GPC framework introduces S_t as an explicitly designed and controlled variable, opening a new optimization dimension that is orthogonal to materials development.

Consider three concrete manifestations of this principle. In battery formation, the SEI growth rate depends exponentially on local overpotential through nucleation kinetics [3,4,7,36]; a temporally structured current that periodically reduces overpotential produces a denser, more uniform SEI film than constant current at the same average rate. In water electrolysis, bubble nucleation and detachment from the electrode surface are threshold phenomena [17,18]; periodic current modulation triggers detachment at controlled intervals, reducing average bubble coverage and cell overpotential by approximately 11%. In electroplating, grain nucleation rate depends nonlinearly on supersaturation [15,16]; high-current bursts create many nucleation sites while subsequent low-current intervals allow diffusion layer recovery, yielding finer grain structure than equivalent DC deposition.

Figure 3. Energy Distribution Principle: Identical Energy, Different Temporal Structure, Different Outcome

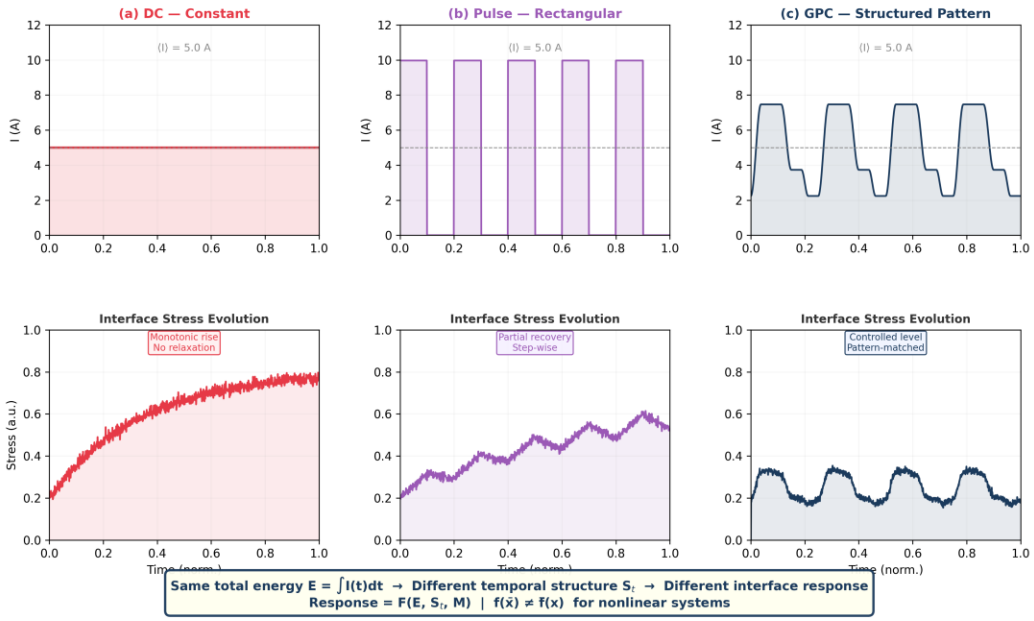

Figure 3. Energy distribution principle. Three current profiles — DC, rectangular pulse, and structured pattern — deliver identical average current and total energy. Resulting interface stress evolution differs fundamentally: DC produces monotonic accumulation, pulse achieves partial recovery, and the structured pattern maintains controlled stress through temporally matched delivery.

The mechanism operates through the multilayer nature of the electrochemical interface [12,13,24]. The double layer responds to high-frequency excitation components (µs–ms), the diffusion layer to mid-frequency components (ms–s), and surface adsorption and catalytic turnover to low-frequency modulation (ms–s). A structured pattern containing components at multiple timescales simultaneously addresses several interfacial processes:

$$E(t) = E_{slow}(t) + E_{mid}(t) + E_{fast}(t) \qquad (6)$$

Each component targets a different interfacial layer. This multi-scale coupling is the mechanism by which temporal structure translates into process outcome differences at constant average current. In multi-source GPC architectures, these frequency components can be generated independently by separate current sources and superposed at the electrode, enabling independent control of energy delivery at different timescales — an approach that has no analog in conventional CC or pulse electrolysis.

Figure 5. Pattern–Interface Multi-Layer Interaction Model

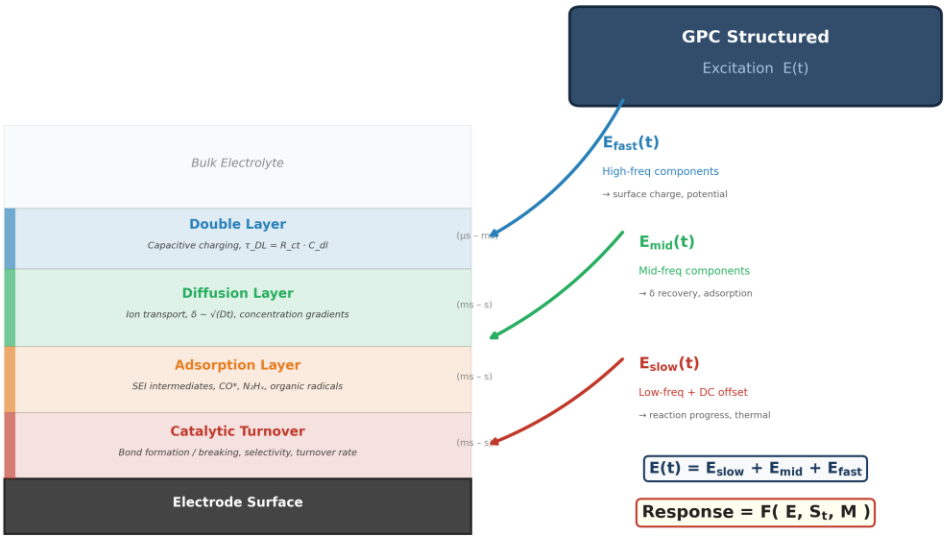

Figure 4. Pattern–interface multi-layer interaction. Structured excitation targets different electrochemical timescales: E_fast for double-layer dynamics, E_mid for diffusion and adsorption, E_slow for catalytic turnover and thermal management. The composite response depends on both total energy and its temporal distribution.

4. Cross-Domain Applicability

The energy distribution principle applies to any electrochemical system with nonlinear interface dynamics. An accompanying paper series demonstrates applicability across more than 15 sectors — including defense, space, and biomedical applications — organized into three groups (Table 1). The common thread is that each domain involves driving a nonlinear electrochemical interface with electrical energy, and in each case the interface dynamics span multiple characteristic timescales that conventional constant-current protocols fail to address independently.

In battery formation, the framework structures SEI growth into three feedback-gated phases — nucleation, consolidation, and stabilization — reducing formation time by 50–70% relative to CC protocols while lowering first-cycle irreversible capacity loss [1,34,37]. In fast charging, pattern delivery keeps the anode lithium concentration gradient below the plating threshold by matching current modulation to solid-state diffusion timescales, extending cycle life at rates exceeding 2C [6,8,10,35,38]. In energy station architecture, multi-source anti-phase coordination reduces grid peak demand by approximately 40% while maintaining per-vehicle charge rates [1].

In hydrogen electrolysis, structured current promotes periodic bubble detachment from electrode surfaces, reducing average bubble coverage and cell overpotential by approximately 11% at equivalent production rates [17,18]. In electroplating, the framework delivers high-nucleation bursts for fine grain formation followed by diffusion-layer recovery intervals that prevent dendritic growth [15,16]. In anodizing, three-phase current cycling (formation–dissolution–thermal stabilization) produces hexagonal self-ordered pore arrays in a single-step process [19,20,21,40].

Conceptual extensions include fusion energy systems, where temporally structured plasma heating power may improve confinement through interaction with nonlinear edge-localized mode dynamics [30,31,32,33], and electrochemical synthesis (CO_2 reduction, nitrogen reduction), where pattern–interface interaction offers selectivity control through multi-timescale management of adsorbed intermediates [24,25,26].

In semiconductor processing, carrier activation through rapid thermal annealing uses constant-temperature profiles that cannot independently control dopant diffusion and defect dynamics. Temporal structuring of the heating profile could decouple these mechanisms [27,28]. In supercapacitor conditioning, pattern delivery during initial charge-discharge cycling enhances electrode wetting and electrolyte penetration into microporous carbon structures [22,23,29,39]. In biomedical applications, neural and muscular stimulation already uses patterned electrical delivery; the GPC framework provides a formal optimization structure for these protocols.

#	Domain	Nonlinear Target	Control	Key Result
1	Battery Formation	SEI nucleation/growth	I(t)	50–70% time reduction
2	Fast Charging / BESS	Li plating threshold	I(t)	Extended cycle life at 2C+
3	Energy Station	Grid-battery coupling	Multi-src	~40% peak demand reduction
4–7	PV / FC / HyCap / Semi	Trap/catalyst/DL kinetics	I(t)	Efficiency, activation
8–9	Plating / Etching	Diffusion layer	I(t)	Surface quality
10	Electrolysis	Bubble dynamics	I(t)	~11% V_cell reduction
11–13	Anodize / Dissolve / Exfol.	Oxide/leveling/intercalation	I(t)	Uniformity, quality
14	Fusion Systems	Plasma instability	P(t)	Confinement (conceptual)
15	Electrochem. Synthesis	Reaction selectivity	E(t)	Faradaic efficiency

Table 1. *Cross-domain applicability of temporal energy structuring. Each domain exhibits nonlinear interface dynamics where temporal structuring affects outcomes beyond what constant-current protocols achieve.*

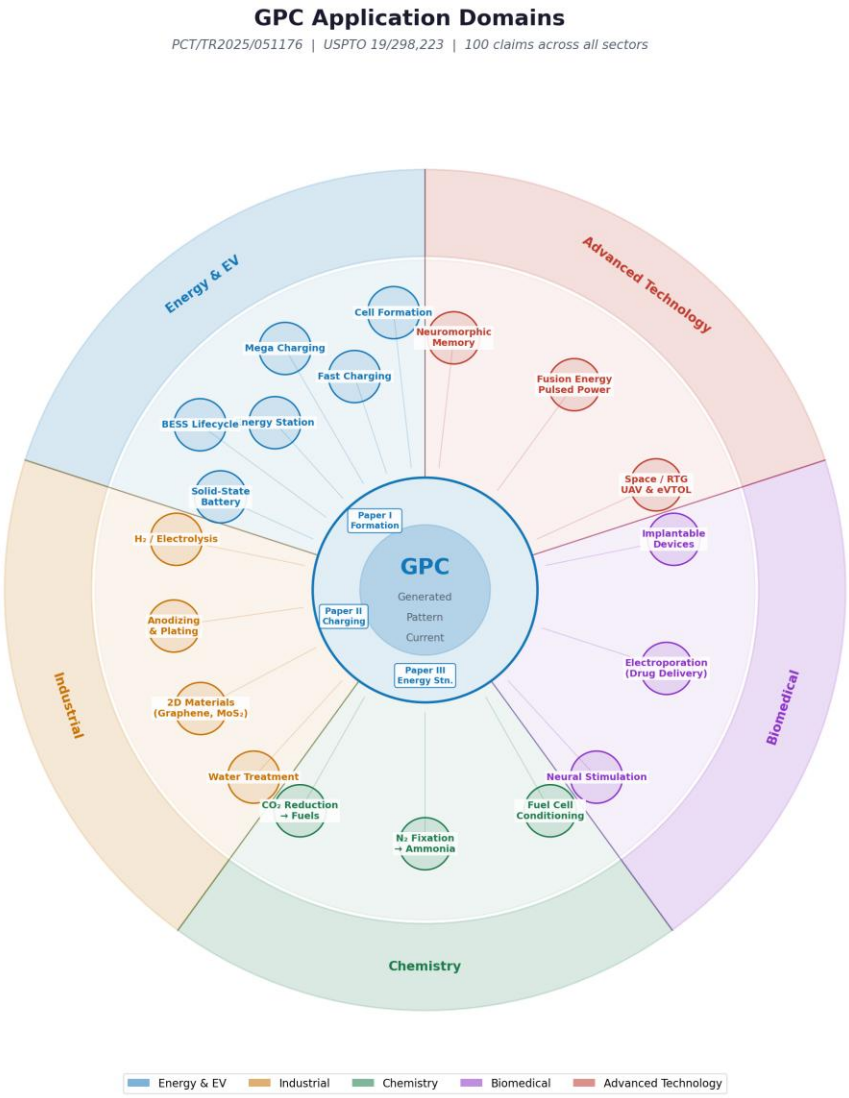

Figure 4. GPC application domain map. Papers I–III cover Energy & EV in detail. All other domains addressed in dedicated publications.

Figure 5. Application domain map spanning Energy & EV, Industrial Electrochemistry, Chemistry, Biomedical, and Advanced Technology sectors. The central principle — temporal energy structure as a control parameter — applies universally across all domains.

5. Outlook and Research Agenda

Experimental validation is the immediate priority: controlled comparisons of CC/CV baselines against GPC protocols at matched average current and total energy, isolating the temporal structure effect. The experimental barrier is deliberately low — the framework requires only a programmable current source with arbitrary waveform capability, implementable as firmware on existing potentiostat and galvanostat platforms. No new cells, electrolytes, or electrode materials are needed [1].

Three research directions are particularly promising. First, data-driven pattern optimization through Bayesian methods or reinforcement learning on impedance feedback may discover

pattern geometries that outperform human-designed templates, analogous to how machine learning has accelerated battery charging protocol design [9,11]. Second, the ChemPat synthesis mode — generating patterns from electrode kinetic parameters — could evolve toward digital twins where the optimal temporal structure is computed from first-principles models before experimental execution. Third, multi-source synchronization at industrial scale (gigafactory formation lines, MW electrolyzers, EV charging stations) represents an engineering challenge with substantial commercial impact.

Industrial adoption faces a deliberately low barrier. The framework is implemented entirely in firmware — the current pattern generator, feedback controller, and stress index calculator run on standard embedded processors. For battery gigafactories operating 200+ formation channels, deploying GPC requires a software update or GP module adaptation to existing formation cyclers. For MW-scale PEM electrolyzers, the power supply already contains programmable current regulation; adding temporal structure is a control algorithm change. This hardware-agnostic characteristic distinguishes the framework from materials-based innovations that require retooling supply chains.

The conceptual extension to non-electrochemical energy-driven nonlinear systems — plasma physics [30,31], semiconductor processing [27,28], biological stimulation — suggests that temporal energy structuring may be a general control principle applicable wherever nonlinear interfaces are driven by electrical energy. If this generalization holds, the framework has implications beyond electrochemistry. The accompanying paper series (Papers 1–15) provides domain-specific theoretical analyses, detailed S_gpc stress modeling, and ChemPat-derived pattern specifications for each application, establishing the experimental protocols for community validation.

Acknowledgments

The technology is protected under PCT/TR2025/051176 and USPTO Application No. 19/298,223 (priority: July 23, 2025). The author is the sole inventor. Companion papers 1–15 provide domain-specific analyses. Preprint available at SSRN (ID: 6387818).

Declaration of Interests

The author declares a financial interest as inventor and developer of the described technology. Ibrahim Karakoc holds commercial rights to the Generated Pattern Current framework.

Declaration of Generative AI in the Writing Process

During the preparation of this work, the author used Claude (Anthropic), ChatGPT (OpenAI), Grok (xAI), and Gemini (Google) for literature review assistance, manuscript drafting, figure generation, and formatting. The author reviewed and edited all content and takes full responsibility for the publication.

References

[1] I. Karakoc, PCT/TR2025/051176; USPTO 19/298,223. Priority: July 23, 2025.
[2] M. Armand, J.-M. Tarascon, Nature 451 (2008) 652–657.
[3] E. Peled, J. Electrochem. Soc. 126 (1979) 2047–2051.
[4] E. Peled, S. Menkin, J. Electrochem. Soc. 164 (2017) A1703–A1719.
[5] J. Vetter et al., J. Power Sources 147 (2005) 269–281.
[6] T. Waldmann, B.-I. Hogg, M. Wohlfahrt-Mehrens, J. Power Sources 384 (2018) 107–124.
[7] S.K. Heiskanen, J. Kim, B.L. Lucht, Joule 3 (2019) 2322–2333.
[8] A. Tomaszewska et al., eTransportation 1 (2019) 100011.
[9] P.M. Attia et al., Nature 578 (2020) 397–402.
[10] C.Y. Wang et al., Nature 611 (2022) 485–490.
[11] K.A. Severson et al., Nat. Energy 4 (2019) 383–391.
[12] A.J. Bard, L.R. Faulkner, Electrochemical Methods, 2nd ed., Wiley, 2001.
[13] J. Newman, K.E. Thomas-Alyea, Electrochemical Systems, 3rd ed., Wiley, 2004.
[14] N. Ibl, Surf. Technol. 10 (1980) 81–104.
[15] M.S. Chandrasekar, M. Pushpavanam, Electrochim. Acta 53 (2008) 3313–3322.
[16] M. Schlesinger, M. Paunovic, Modern Electroplating, 5th ed., Wiley, 2010.
[17] M. Carmo et al., Int. J. Hydrogen Energy 38 (2013) 4901–4934.
[18] H. Vogt, R.J. Balzer, Electrochim. Acta 50 (2005) 2073–2079.
[19] H. Masuda, K. Fukuda, Science 268 (1995) 1466–1468.
[20] D. Landolt, Electrochim. Acta 32 (1987) 1–11.
[21] M. Datta, D. Landolt, Electrochim. Acta 45 (2000) 2535–2558.
[22] K.S. Novoselov et al., Science 306 (2004) 666–669.
[23] K. Parvez et al., J. Am. Chem. Soc. 136 (2014) 6083–6091.
[24] S. Nitopi et al., Chem. Rev. 119 (2019) 7610–7672.
[25] S.Z. Andersen et al., Nature 570 (2019) 504–508.
[26] M. Yan, Y. Kawamata, P.S. Baran, Chem. Rev. 117 (2017) 13230–13319.
[27] S.M. Sze, K.K. Ng, Physics of Semiconductor Devices, 3rd ed., Wiley, 2007.
[28] T. Kimoto, J.A. Cooper, Fundamentals of Silicon Carbide Technology, Wiley, 2014.
[29] B.E. Conway, Electrochemical Supercapacitors, Springer, 1999.
[30] J. Wesson, Tokamaks, 4th ed., Oxford University Press, 2011.
[31] J.P. Freidberg, Plasma Physics and Fusion Energy, Cambridge University Press, 2007.
[32] T.E. Evans et al., Phys. Rev. Lett. 92 (2004) 235003.
[33] A. Loarte et al., Plasma Phys. Control. Fusion 45 (2003) 1549–1569.
[34] S.J. An et al., J. Power Sources 342 (2017) 846–852.
[35] P.H.L. Notten, J.H.G. Op het Veld, J.R.G. van Beek, J. Power Sources 145 (2005) 89–94.
[36] M. Winter, Z. Phys. Chem. 223 (2009) 1395–1406.
[37] F. Schomburg et al., Energy Environ. Sci. 17 (2024) 2686–2733.
[38] P.E. de Jongh, P.H.L. Notten, Solid State Ionics 148 (2002) 259–268.
[39] Z. Yang et al., Chem. Rev. 111 (2011) 3577–3613.
[40] O. Jessensky, F. Muller, U. Gosele, Appl. Phys. Lett. 72 (1998) 1173–1175.